The Company of **Biologists**

RESEARCH ARTICLE

The Egalitarian binding partners Dynein light chain and Bicaudal-D act sequentially to link mRNA to the Dynein motor

Chandler H. Goldman, Hannah Neiswender, Rajalakshmi Veeranan-Karmegam and Graydon B. Gonsalvez*

ABSTRACT

A conserved mechanism of polarity establishment is the localization of mRNA to specific cellular regions. Although it is clear that many mRNAs are transported along microtubules, much less is known about the mechanism by which these mRNAs are linked to microtubule motors. The RNA binding protein Egalitarian (Egl) is necessary for localization of several mRNAs in *Drosophila* oocytes and embryos. Egl also interacts with Dynein light chain (Dlc) and Bicaudal-D (BicD). The role of Dlc and BicD in mRNA localization has remained elusive. Both proteins are required for oocyte specification, as is Egl. Null alleles in these genes result in an oogenesis block. In this report, we used an shRNA-depletion strategy to overcome the oogenesis block. Our findings reveal that the primary function of Dlc is to promote Egl dimerization. Loss of dimerization compromises the ability of Egl to bind RNA. Consequently, Egl is not bound to cargo, and is not able to efficiently associate with BicD and the Dynein motor. Our results therefore identify the key molecular steps required for assembling a localization-competent mRNP.

KEY WORDS: RNA localization, Molecular motor, Kinesin, Cell polarity, Cargo adaptor, *Drosophila*

INTRODUCTION

Recent studies have shown that mRNA localization is a prevalent, potent and conserved mechanism used by cells to regulate protein sorting (Lecuyer et al., 2007; Mili et al., 2008; Cajigas et al., 2012; Ryder and Lerit, 2018). Although there are several pathways by which mRNAs are localized, active motor-based transport along cytoskeletal filaments is a commonly used mechanism. In *Drosophila* oocytes and embryos, numerous mRNAs are localized to distinct intracellular sites (Goldman and Gonsalvez, 2017). For many of these mRNAs, localization requires the activity of the minus end-directed microtubule motor, cytoplasmic Dynein (hereafter referred to as Dynein) (Kardon and Vale, 2009; Suter, 2018). The mechanism by which Dynein is able to bind these mRNAs in the complex and crowded environment of the cell is unknown.

Egalitarian (Egl) is an RNA binding protein that associates with several mRNAs that are localized in a Dynein-dependent manner (Dienstbier et al., 2009). Egl also interacts with Dynein light chain/LC8 (Dlc; also known as Cdlc1 and Ctp) and Bicaudal-D (BicD) (Mach and Lehmann, 1997; Navarro et al., 2004). Dlc is a component of the Dynein motor and BicD interacts with Dynactin, a crucial regulator of Dynein (Hoogenraad et al., 2001; Rapali et al.,

Cellular Biology and Anatomy, Medical College of Georgia, Augusta University, 1459 Laney Walker Blvd, Augusta, GA 30912, USA.

*Author for correspondence (ggonsalvez@augusta.edu)

G.B.G., 0000-0002-4458-8497

2011). BicD is thought to stabilize the interaction between Dynactin and Dynein, thereby promoting processive movement of the motor complex (McKenney et al., 2014; Schlager et al., 2014). Thus, in theory, both of the Egl binding partners are capable of linking mRNA-bound Egl with the Dynein motor. Recent *in vitro* studies have shown that a minimal complex consisting of RNA, Egl, BicD, Dynactin and Dynein is sufficient for transport (McClintock et al., 2018; Sladewski et al., 2018). Whether or not this complex is sufficient for mRNA localization *in vivo*, however, is not known.

Egl, Dlc, BicD and components of the Dynein motor are required for oocyte specification (Mach and Lehmann, 1997; McGrail and Hays, 1997; Navarro et al., 2004). Null mutants in these genes result in an oogenesis block. As such, mRNA localization, which is primarily studied in mid- and late-stage egg chambers and early embryos, cannot be analyzed using null alleles. We recently overcame this limitation by using an shRNA depletion strategy (Sanghavi et al., 2016). This approach revealed an essential role for Egl in the localization of *oskar* (*osk*), *bicoid* (*bcd*) and *gurken* (*grk*) mRNAs (Sanghavi et al., 2016). In this study, we used a similar strategy to define the mechanism by which Egl, Dlc and BicD function to link mRNAs with Dynein. Our results reveal a step-wise assembly pathway for building a localization-competent mRNP.

RESULTS

Egl contains binding sites for BicD and Dlc on opposite ends of the protein and a central region that is essential for RNA binding (Fig. 1A) (Mach and Lehmann, 1997; Navarro et al., 2004; Dienstbier et al., 2009). Point mutations have been identified within Egl that disrupt either Dlc or BicD binding. For example, the *egl2pt* allele contains two mutations that disrupt Dlc interaction (Navarro et al., 2004). The *egl4e* allele contains a single mutation that compromises BicD binding (Mach and Lehmann, 1997). However, as with null alleles of *egl*, flies that are homozygous for *egl2pt* or *egl4e* fail to specify an oocyte (Mach and Lehmann, 1997; Navarro et al., 2004). Consequently, the effects of these mutations on mRNA localization could not be studied.

In order to overcome this early requirement for Egl, we developed an shRNA depletion strategy (Sanghavi et al., 2016). By expressing an shRNA against *egl* using a stage-specific driver, we were able to generate egg chambers that were depleted of Egl within the germline. We reasoned that we could use a similar approach to address the functional role of the Egl/Dlc and Egl/BicD interactions. Transgenes were generated that encode either wild-type *egl* (*egl_wt*), *egl_2pt* or *egl_4e*. The constructs were tagged on the C-terminus with RFP and contained silent mutations that made them refractory to the *egl* shRNA. All three transgenes were integrated at the same genomic locus and brought into the background of the *egl* shRNA strain. Thus, we were able to generate flies that were depleted of endogenous Egl, but expressed either wild-type or mutant versions of Egl in mid to late stage egg chambers and early embryos.
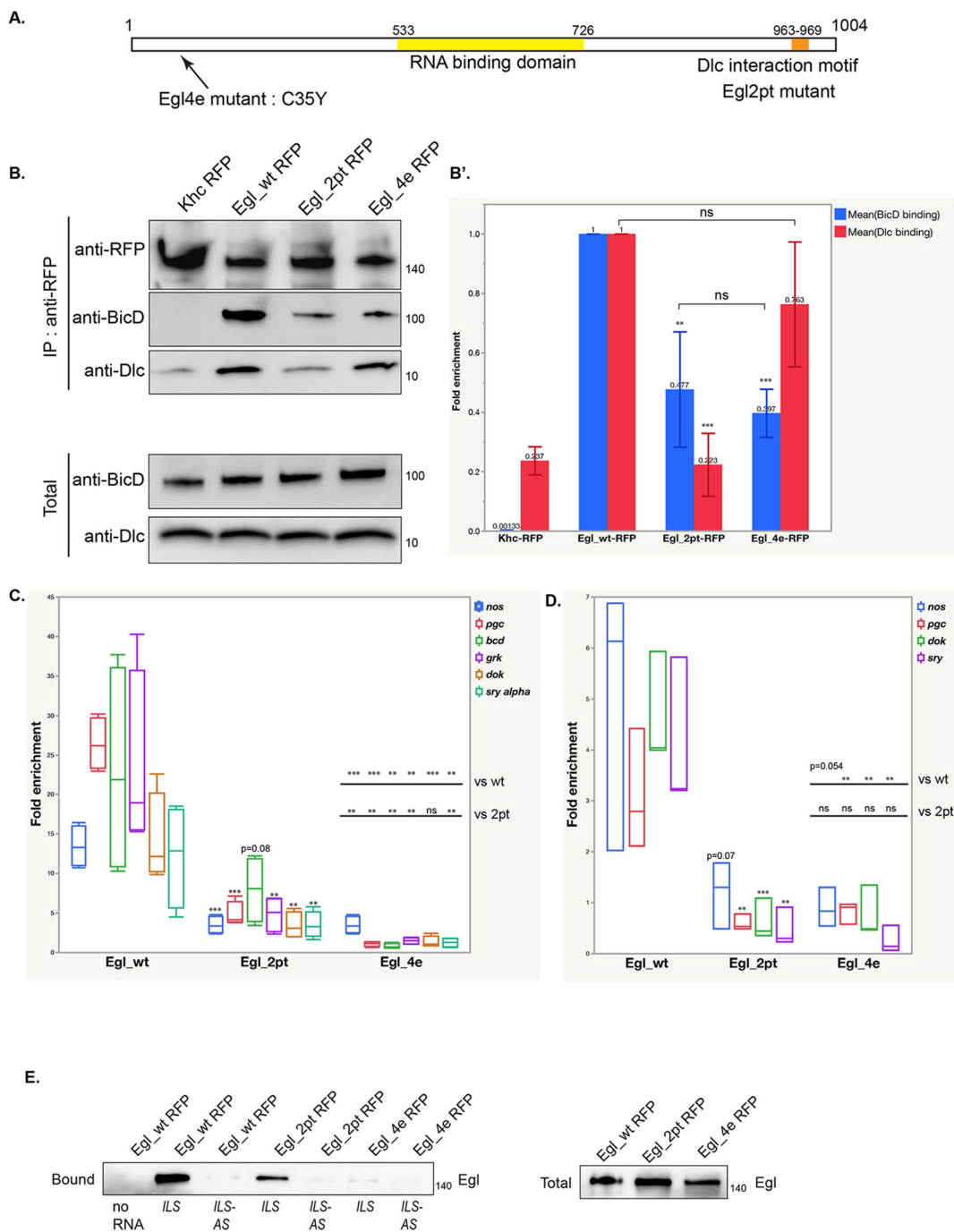
Fig. 1. Egl_2pt and Egl_4e are deficient for binding RNA. (A) Schematic illustrating the domain structure of Egl. The RNA binding domain, the position of Egl_4e (C35Y) and the Dlc binding domain are indicated. Egl_2pt contains two mutations within this region, S965K and S969R. (B) Western blot analysis of co-immunoprecipitation using ovarian lysates from strains expressing Khc-RFP, Egl_wt-RFP, Egl_2pt-RFP or Egl_4e-RFP. The strains expressing the Egl transgenes were also depleted of endogenous Egl. (B′) The binding results from four different biological replicates were quantified. The values for BicD and Dlc were normalized to the level of co-precipitation of these proteins with wild-type Egl. In order to validate the linear range and sensitivity of our imaging system, a titration of ovarian lysate was analyzed using the antibody against Dlc and BicD (Fig. S1B,C). (C,D) Bound RNA from ovarian lysates (C) or 0 to 8 h embryonic lysates (D) from identical crosses were analyzed by RT-qPCR. In comparison with wild-type, Egl_2pt and Egl_4e were compromised for binding the indicated RNA cargoes in ovaries (four biological replicates) and embryos (three biological replicates). *grk* and *bcd* mRNAs were not highly enriched in Egl pellets in the embryo, so are not included in D. To calculate fold enrichment, the indicated mRNAs were normalized to the amount of γ-tubulin in each pellet. Boxes in C indicate the 75%, 50% and 25% and whiskers indicate outliers. Boxes in D indicate maximum value, median value and and minimum value. (E) Western blot analysis of *ILS* or *ILS-AS* binding to strains expressing Egl_wt-RFP, Egl_2pt-RFP or Egl_4e-RFP depleted of endogenous Egl. A total fraction is also shown. Egl_2pt and Egl_4e are both defective for binding *ILS*. Data are mean±s.d. ***P<0.001, **P<0.05 (unpaired *t*-test). ns, not significant.

As expected, Egl_wt interacted efficiently with BicD and Dlc (Fig. 1B). Also as expected, Egl_4e was able to bind Dlc but was deficient for BicD binding (Fig. 1B,B′). Consistent with published results (Navarro et al., 2004), Egl_2pt was compromised for Dlc binding (Fig. 1B,B′, Fig. S1B,C). Unexpectedly, this mutant was also deficient for binding BicD

(Fig. 1B,B′, Fig. S1B,C). A similar result was obtained by performing this experiment in *Drosophila* S2 cells (Fig. S1A). Thus, point mutations within the Dlc-interaction motif somehow also affect the Egl/BicD interaction.

We next examined the ability of these mutants to interact with native mRNAs. Ovarian or embryonic lysates were prepared from flies expressing wild-type or mutant RFP-tagged Egl. A strain expressing RFP-tagged Kinesin heavy chain (Khc) was used as a negative control. Lysates were incubated with RFP-trap beads, the co-precipitating RNAs were extracted and analyzed by reverse transcription followed by quantitative PCR. *bcd* and *grk* mRNAs are known targets of Egl (Bullock and Ish-Horowicz, 2001; Dienstbier et al., 2009), whereas *nanos* (*nos*), *polar granule component* (*pgc*), *dok* and *sry alpha* (*sry-α*) were recently identified as Egl cargoes using RIP-seq (Vazquez-Pianzola et al., 2017). In contrast to wild-type, Egl_2pt and Egl_4e were defective for binding mRNA cargo in ovaries and embryos (Fig. 1C,D). For several of the cargoes examined in ovarian lysates, the binding of Egl_4e was significantly more compromised than Egl_2pt (Fig. 1C). For reasons that are unclear, this difference was less apparent in embryonic lysates (Fig. 1D).

In order to validate this result, we examined the ability of wild-type or mutant Egl to bind to a localization element from the *I* factor retrotransposon (*ILS*; *I-element\gag*). The anti-sense version of *ILS* (*ILS-AS*) was used as a control for specificity. *ILS* and *ILS-AS* containing a streptavidin binding apatamer were bound to beads as previously described (Dienstbier et al., 2009). Ovarian lysates were then incubated with the RNA-bound beads. Bound proteins were analyzed using western blotting. Consistent with results obtained using native mRNAs, wild-type Egl efficiently associated with *ILS*, but showed minimal binding to *ILS-AS* (Fig. 1E). By contrast, Egl_2pt displayed reduced binding to *ILS* yet was able to distinguish between *ILS* and *ILS-AS* (Fig. 1E), whereas Egl_4e displayed greatly reduced binding to both *ILS* and *ILS-AS* (Fig. 1E).

Collectively, these results suggest that compromising the ability of Egl to interact with Dlc and BicD also affects its ability to bind RNA. Previous studies have shown that BicD is required for Egl to specifically bind RNA localization sequences (Dienstbier et al., 2009). Thus, the inability of Egl4e to bind RNA is not entirely surprising. However, a role for Dlc in mediating Egl mRNA binding has not been reported.

Although Dlc is a component of the Dynein motor, it also interacts with many proteins in a Dynein-independent manner (Rapali et al., 2011). The available evidence suggests that one of the main functions of Dlc is to facilitate dimerization or oligomerization of proteins (Barbar, 2008). In this regard, Egl has been shown to exist as a dimer in ovarian lysates (Mach and Lehmann, 1997). We therefore hypothesized that Dlc is required for Egl dimerization, and that dimerization is a pre-requisite for efficient RNA binding. In addition, although Egl and BicD can directly interact, the Bullock and Trybus labs recently demonstrated that this interaction is greatly enhanced by RNA (McClintock et al., 2018; Sladewski et al., 2018). Thus, we further posit that by affecting the ability of Egl to bind RNA, loss of dimerization also affects its ability to interact with BicD.

In order to test this hypothesis, we immunoprecipitated wild-type or mutant RFP-tagged Egl in strains that also expressed endogenous Egl. Consistent with previous results (Mach and Lehmann, 1997), Egl_wt-RFP was able to co-precipitate endogenous Egl (Fig. 2A). A similar result was obtained for Egl_4e-RFP. Consistent with our hypothesis, Egl_2pt-RFP was unable to co-precipitate endogenous Egl (Fig. 2A). In order to test dimerization more directly, we co-expressed GFP and FLAG versions of wild-type or mutant Egl in S2 cells. Whereas wild-type Egl-GFP was able to co-precipitate

wild-type Egl-FLAG, Egl_2pt-GFP was unable to co-precipitate Egl_2pt-FLAG (Fig. 2B). We therefore conclude that Egl_2pt is dimerization defective. We further demonstrate that Egl dimerization is independent of its RNA binding activity. An Egl construct lacking the RNA binding domain was able to dimerize and interact with Dlc (Fig. S1D and Fig. 2C). As expected given recent findings (McClintock et al., 2018; Sladewski et al., 2018), loss of RNA binding significantly compromised the Egl-BicD interaction (Fig. 2C).

The above experiments involve a mutant of Egl that is defective for Dlc binding. If our hypothesis is correct, we should obtain similar results by depleting Dlc. Genetic loss of Dlc is lethal and germline clones do not specify an oocyte (Dick et al., 1996; Navarro et al., 2004). We therefore attempted to deplete Dlc using a specific shRNA and the same driver that was successful in depleting Egl (Sanghavi et al., 2016). Unfortunately this resulted in an oogenesis block (Fig. S1E,E′). We therefore used a different maternal driver that is expressed in slightly later stage egg chambers (Sanghavi et al., 2016). Although Dlc could be depleted using this driver, the knockdown was incomplete (Fig. 2D). Consistent with our hypothesis, depletion of Dlc partially compromised the ability of Egl to interact with RNA and BicD (Fig. 2D,D′,E). The binding deficit observed with this strategy is not as strong as that observed in the Egl_2pt background. We attribute this difference to the incomplete depletion of Dlc using this driver and shRNA combination.

These findings raise an important question. Is the role of Dlc in this pathway simply to mediate Egl dimerization? If this is true, we might be able to bypass the function of Dlc by artificially dimerizing Egl. We tested this hypothesis using S2 cells. Sladewski and colleagues used a leucine zipper to artificially dimerize a truncated version of Egl (Sladewski et al., 2018). Using a similar approach, we observed that, although Egl_2pt does not dimerize, Egl_2pt containing a C-terminal leucine zipper efficiently dimerizes (Fig. 3A, Egl_2pt-zip). As expected, Egl_2pt-zip was still unable to bind Dlc. However, despite this inability, Egl_2pt-zip was able to interact with BicD (Fig. 3B).

We next examined RNA binding using Egl_wt or Egl_2pt constructs that contained or lacked the leucine zipper. Egl_wt and Egl_wt-zip were both able to bind strongly to *ILS* and were able to distinguish *ILS* from *ILS-AS* (Fig. 3C,C′). As expected, Egl_2pt had a reduced affinity for *ILS* in comparison with Egl_wt (Fig. 3C,C′). Consistent with our hypothesis, the binding affinity for *ILS* was restored with Egl_2pt-zip (Fig. 3C,C′). Similar results were obtained using *TLS* [*fs(1)K10*], the localization element from *K10* mRNA (Fig. S1F). Thus, RNA binding activity is restored upon artificial dimerization of Egl. Based on these results, we conclude that the primary function of Dlc in this pathway is to mediate Egl dimerization. Once dimerization is restored, RNA and BicD binding are also restored.

If Egl is unable to bind BicD, its association with the Dynein motor will likely also be compromised. Although the Egl/BicD/ Dynein complex can be reconstituted using purified components (McClintock et al., 2018; Sladewski et al., 2018), the existence of this complex in native ovarian lysates has been difficult to demonstrate. McClintock and colleagues were able to co-precipitate a small amount of Dynein heavy chain (Dhc, the motor subunit of Dynein; also known as Dhc64C) with Egl from ovarian lysates only upon addition of excess RNA cargo (McClintock et al., 2018). Because Egl_2pt and Egl_4e are deficient for binding RNA, a different strategy is needed to analyze the *in vivo* association of these mutants with Dynein. We chose to pursue a localization approach to study this.
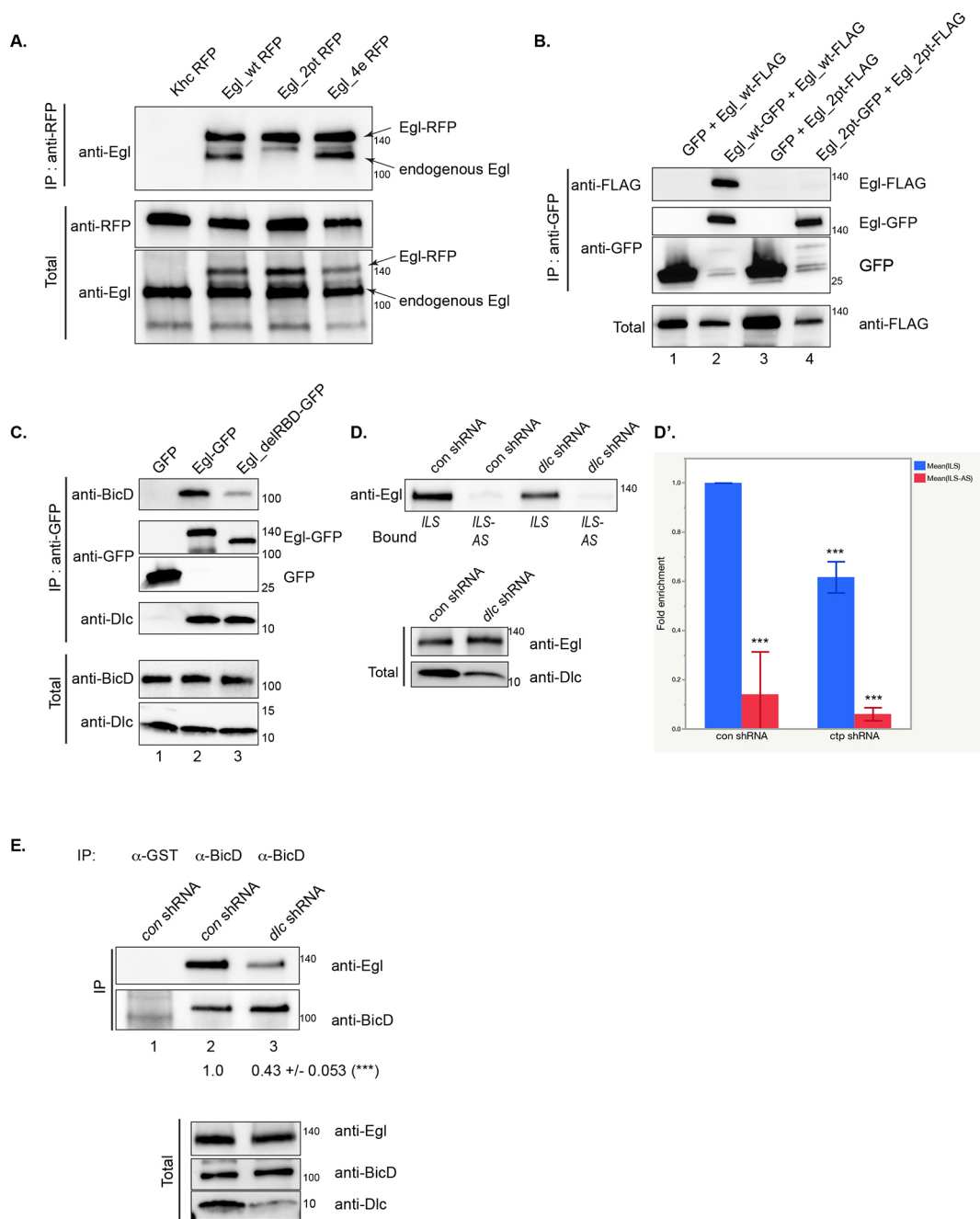
Fig. 2. Dlc is required for Egl dimerization. (A) Western blot analysis of co-immunoprecipitation using ovarian lysates prepared from strains expressing Khc-RFP, Egl_wt-RFP, Egl_2pt-RFP or Egl_4e-RFP. The strains also expressed endogenous Egl. The total fraction is shown. Egl_wt-RFP and Egl_4e-RFP were able to co-precipitate endogenous Egl, whereas Khc-RFP and Egl_2pt-RFP were not. (B) Co-precipitation using S2 cells transfected with: GFP and Egl_wt-FLAG, Egl_wt-GFP and Egl_wt-FLAG, GFP and Egl_2pt-FLAG, and Egl_2pt-GFP and Egl_2pt-FLAG. The total fraction is shown. Egl_2pt is dimerization defective. (C) Co-precipitation using S2 cells transfected with: GFP, Egl_wt-GFP, and Egl_delRBD-GFP (an Egl construct lacking the RNA binding domain). Bound and total fractions are shown. Deletion of the RNA binding domain compromises the Egl-BicD interaction but not the Egl-Dlc interaction. (D) Western blot analysis of *ILS* or *ILS-AS* binding in ovarian lysate preparations from strains expressing a control shRNA against the *white* gene (con shRNA) or an shRNA against *dlc*. The total fraction is also shown. (D′) The amount of Egl in the respective pellets was quantified from four independent biological replicates. Values were normalized to the level of Egl detected in the *ILS* fraction from the control sample. Depletion of Dlc compromises the ability of Egl to associate with *ILS*. (E) Western blot analysis of co-immunoprecipitation using either an antibody against GST or BicD. Bound and total fractions are shown. The amount of Egl that co-precipitated with BicD was quantified from three independent biological replicates. The values were normalized to the level of co-precipitating Egl in the control sample and to the level of BicD that was immunoprecipitated under each condition. Depletion of Dlc reduces the Egl-BicD interaction. Data are mean±s.d. ***$P<0.001$ (unpaired t-test).

Dissected ovaries were incubated with a PIPES buffer that enabled the visualization of microtubule filaments with greater clarity (Cho et al., 2016; Veeranan-Karmegam et al., 2016). The ovaries were subsequently fixed and examined for Egl-RFP and microtubule localization. The microtubule lattice was visualized using an antibody against α-tubulin. Significant co-localization was observed between Egl_wt-RFP and microtubules (Fig. 4A,B,C). This pattern was especially prominent in nurse cells (Fig. 4A′,B′,C′).
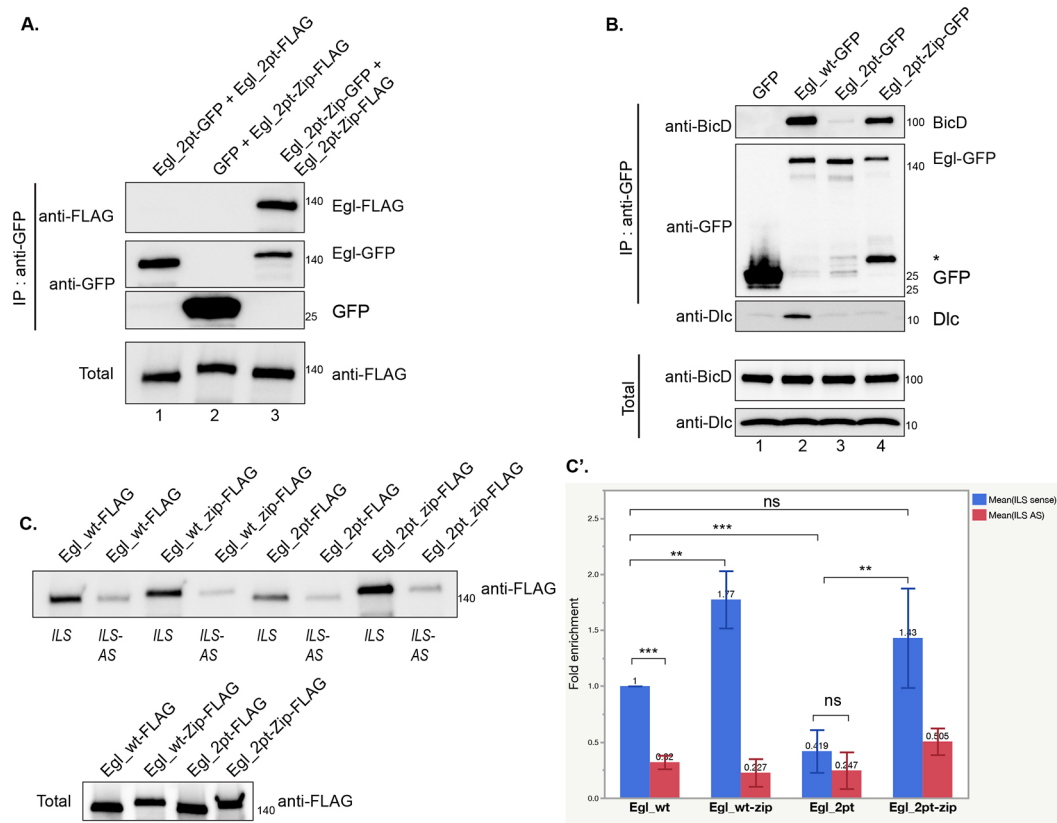
DEVELOPMENT

4

Fig. 3. Artificial dimerization of Egl_2pt restores RNA and BicD binding. (A) Western blot analysis of co-precipitation using S2 cells transfected with: Egl_2pt-GFP and Egl_2pt-FLAG, GFP and Egl_2pt-Zip-FLAG, and Egl_2pt-Zip-GFP and Egl_2pt-Zip-FLAG. Zip refers to a leucine zipper motif. Insertion of the leucine zipper restores Egl_2pt dimerization. (B) Co-precipitation using S2 cells transfected with: GFP, Egl_wt-GFP, Egl_2pt-GFP and Egl_2pt-Zip-GFP. Egl_2pt-Zip-GFP is able to associate with BicD. Asterisk indicates a degradation product that is consistently seen in the Egl_2pt-Zip-GFP lane. (C) Western blot analysis of *ILS* or *ILS-AS* binding in S2 cell lysates expressing the indicated constructs. The bound proteins were analyzed by blotting using the FLAG antibody. A total fraction is also shown. (C′) The amount of Egl that co-precipitated with the RNA-bound beads was quantified from four independent biological replicates. Values were normalized to the level of Egl_wt that co-precipitated with *ILS* and to the expression level of the respective construct in the total lysate. RNA binding activity is restored with Egl_2pt-zip. Data are mean±s.d. ***P<0.001, **P<0.05 (Unpaired *t*-test). ns, not significant.

Microtubule filaments in the oocyte were smaller and thus their potential co-localization with Egl_wt-RFP was harder to ascertain (Fig. 4A″,B″,C″). In contrast to Egl_wt-RFP, Egl_2pt-RFP and Egl_4e-RFP were more diffusely distributed in nurse cells, with only residual filament localization (Fig. 4D-G, arrows). Based on this analysis, we conclude that the ability of Egl_2pt and Egl_4e to associate with microtubules is compromised. It is very likely that the recruitment of Egl to microtubule tracks is mediated by Dynein. However, the monoclonal antibody against Dhc did not consistently reveal a filament localization pattern under these permeabilization and fixation conditions (data not shown). As such, we were not able to directly address this possibility.

Next, we examined the localization of Egl, Dynein and BicD within the oocyte using standard fixation conditions. Wild-type Egl, Dhc and BicD were all enriched in the oocyte of early-stage egg chambers (Fig. 5A,G, Fig. S2E) (Li et al., 1994; Mach and Lehmann, 1997). By contrast, Egl_2pt and Egl_4e were diffusely distributed with little oocyte enrichment (Fig. 5C,E,G). A similar, albeit weaker, phenotype was observed for Dhc and BicD in these egg chambers (Fig. 5C′,E′,G, Fig. S2F,G). The oocyte localization of BicD depends on Egl (Mach and Lehmann, 1997). Thus, one explanation for the weaker localization defect observed for Dhc and BicD in these mutant backgrounds is that, at this stage of development, endogenous Egl is not yet completely depleted (Sanghavi et al., 2016). As such, the partial oocyte enrichment of

Dhc and BicD in these mutants is likely to be mediated by this residual endogenous Egl.

In stage 10 egg chambers expressing wild-type Egl, Dhc was partially enriched at the posterior pole, whereas Egl and BicD were localized to the oocyte cortex (Fig. 5B, Fig. S2H). A similar pattern was observed in egg chambers expressing Egl_2pt (Fig. 5D, Fig. S2I). Thus, although the localization of these factors within the oocyte is defective in early-stage Egl_2pt egg chambers, they are restored to a normal pattern by stage 10. By contrast, all three proteins were significantly delocalized in stage 10 egg chambers expressing Egl_4e (Fig. 5F, Fig. S2J).

Knockdown of Egl results in profound defects in the organization of oocyte microtubules (Sanghavi et al., 2016). We therefore examined microtubule organization in strains expressing Egl_2pt and Egl_4e. Kinesin-β-galactosidase (kinesin-β-gal) localization was used to reveal the distribution of microtubule plus ends, whereas gamma tubulin serves as a marker for minus ends (Clark et al., 1994; Cha et al., 2002). This analysis revealed that, whereas plus and minus ends were correctly localized in egg chambers expressing wild-type Egl and Egl_2pt, both markers were delocalized in mutants expressing Egl_4e (Fig. 6A-F). The oocyte nucleus, which localizes to the dorsal-anterior region in a microtubule-dependent manner (Zhao et al., 2012), was correctly localized in strains expressing wild-type Egl and Egl_2pt, but was sometimes delocalized in egg chambers expressing Egl_4e
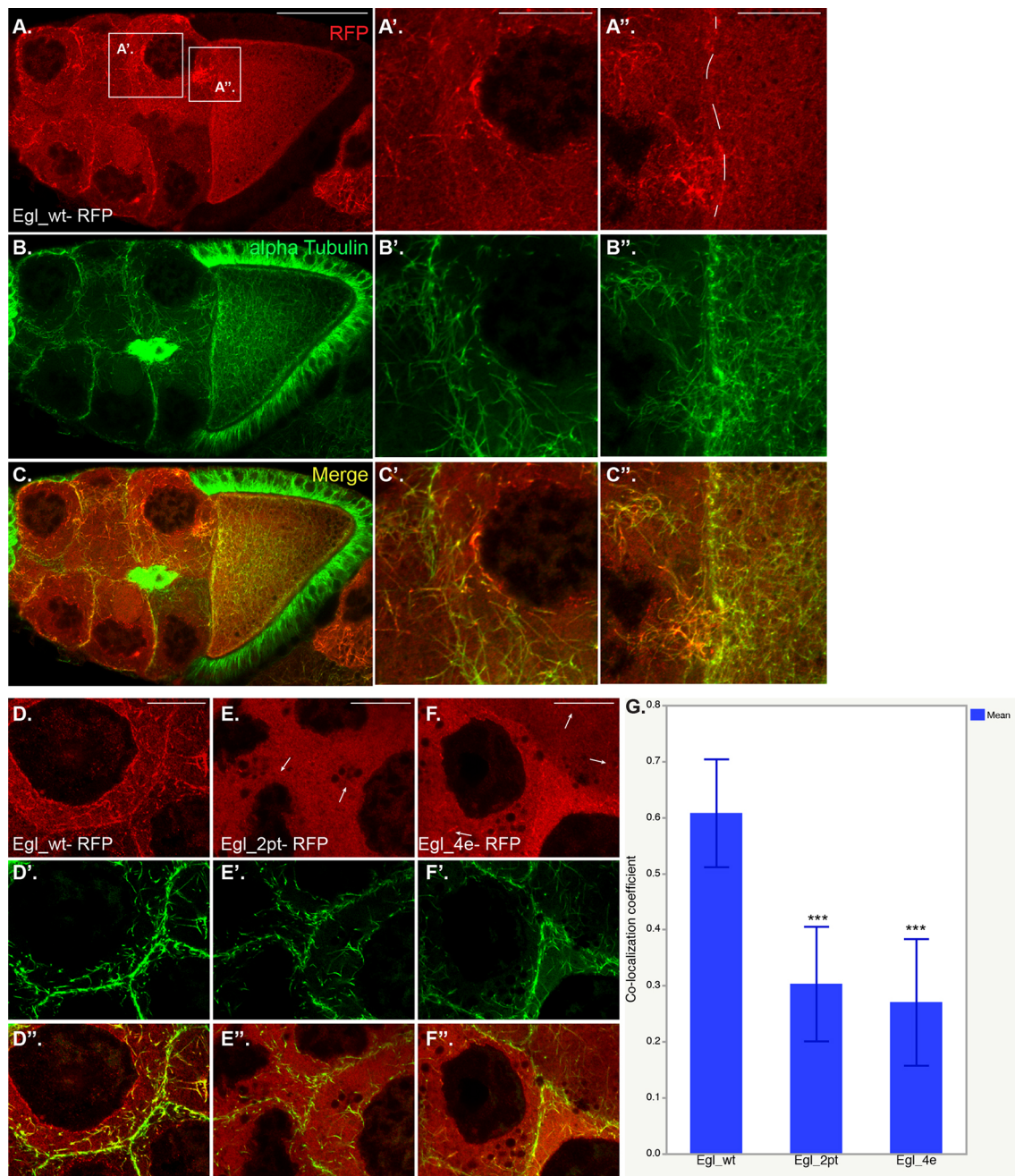
Fig. 4. Filament localization of Egl. (A-F″) Ovaries from flies expressing Egl_wt-RFP (A-D), Egl_2pt-RFP (E) or Egl_4e-RFP (F) and depleted of endogenous Egl. Egg chambers were processed using a polyclonal antibody against RFP (red) and an anti-α-tubulin antibody directly conjugated with FITC (B, green). A merged image is also shown (C, yellow). Magnified views of the boxed regions in A are shown in A′,B′,C′ and A″,B″,C″. The region to the left of the dashed line in A″ corresponds to nurse cell cytoplasm. The region to the right of this line corresponds to oocyte cytoplasm. (G) The co-localization co-efficient between Egl-RFP and microtubules was calculated using 15 egg chambers for each genotype. Significant co-localization is observed between Egl_wt-RFP in nurse cells and microtubule filaments (A-D, G). Egl_2pt-RFP and Egl_4e-RFP display a more diffuse localization with only residual filament localization (E,F, arrows). Data are mean±s.d. ***P<0.001 (unpaired t-test). Scale bars: 50 μm in A-C; 25 μm in D-F.

(Fig. 6G-I). Thus, microtubule organization is preserved in Egl_2pt mutants but is disrupted in Egl_4e mutants. Given that both mutants are deficient for binding BicD and RNA, it is unclear why microtubules are disorganized in the Egl_4e background.

We next examined mRNA localization. The localization of osk mRNA at the posterior of stage 10 egg chambers (Ephrussi et al., 1991; Kim-Ha et al., 1991) was maintained in wild-type Egl and Egl_2pt mutants. However, osk was significantly delocalized in mutants expressing Egl_4e (Fig. 7A-C). The delocalization of osk

mRNA in Egl_4e mutants likely results from the disorganized microtubule cytoskeleton present in these egg chambers.

grk mRNA is enriched in the oocyte of early-stage egg chambers and is localized at the dorsal-anterior cortex by stage 10 (Neuman-Silberberg and Schupbach, 1993). As expected, given the compromised localization of Egl and Dhc in early-stage egg chambers (Fig. 5C,E), the oocyte enrichment of grk was reduced in egg chambers expressing Egl_2pt and Egl_4e (Fig. 7D-F). Furthermore, in comparison with wild-type, the dorsal-anterior
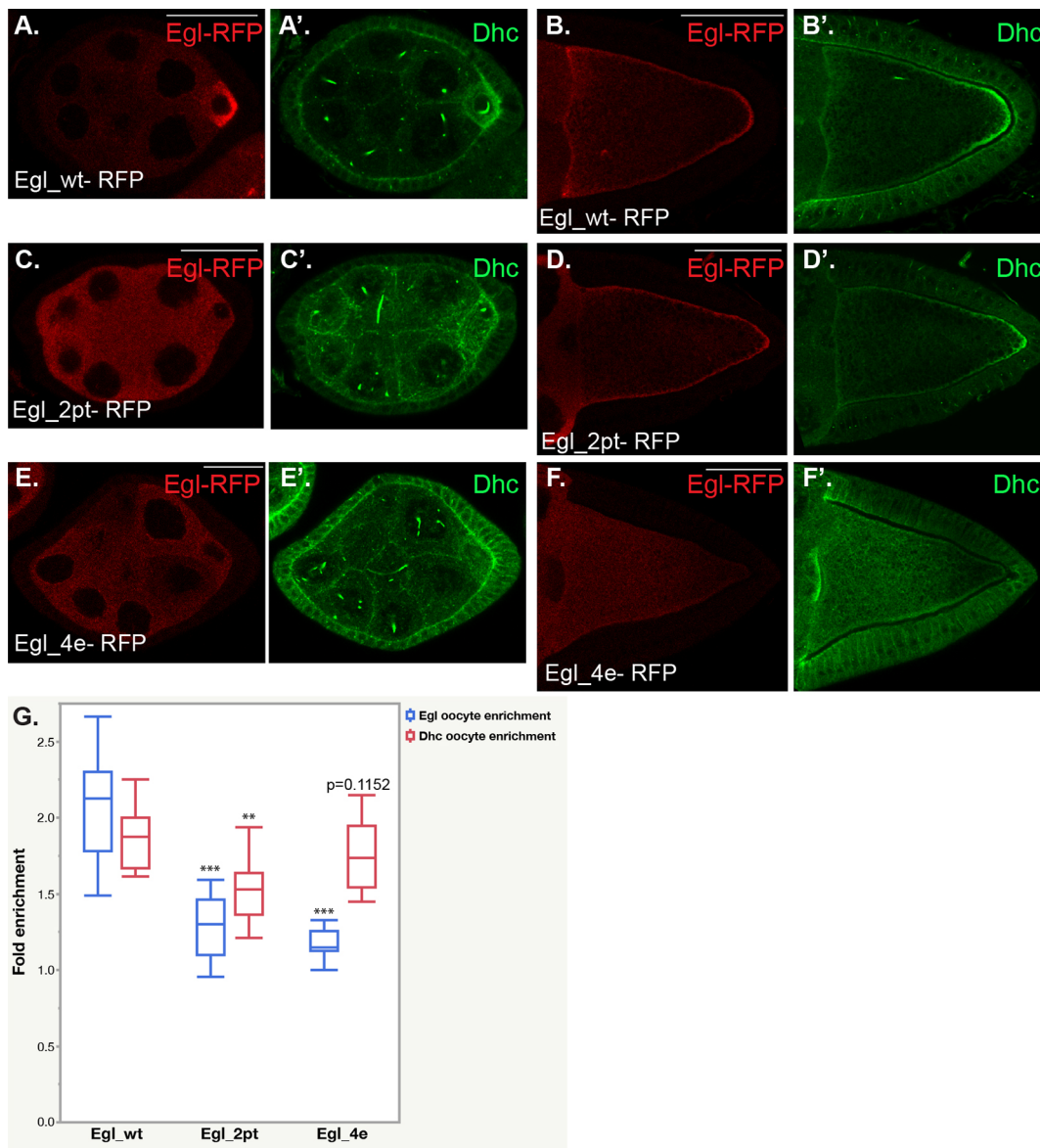
Fig. 5. Oocyte localization of Egl and Dynein. (A-F′) Ovaries from strains expressing Egl_wt-RFP (A,B), Egl_2pt-RFP (C,D) or Egl_4e-RFP (E,F) and depleted of endogenous Egl were fixed and processed using antibodies against RFP (A-F, red) and Dhc (A′-F′, green). Stage 5 (A,C,E) and stage 10 (B,D,F) egg chambers are depicted. (G) The oocyte enrichment of Egl and Dhc in stage 5 egg chambers was quantified. Boxes indicate 75%, 50% and 25% values and whiskers indicate outliers. Data are mean±s.d. n=15, ***P<0.001, **P<0.05 (unpaired t-test). Scale bars: 25 µm in A,C,E; 50 µm in B,D,F.

enrichment of *grk* mRNA was reduced in Egl_2pt mutants and was completely abrogated in Egl_4e egg chambers (Fig. 7D′-F′,J). Grk protein, produced at the dorsal corner of the oocyte, is secreted and signals the overlying follicle cells to adopt dorsal fate (Neuman-Silberberg and Schupbach, 1993). The end result is formation of dorsal appendages in mature eggs. Consistent with the mRNA localization result, normal dorsal appendage formation was reduced in Egl_2pt mutants and was severely compromised in Egl_4e flies (Fig. 7K).

bcd mRNA localizes at the anterior margin of stage 10 egg chambers where it persists until early stages of embryogenesis (Berleth et al., 1988). As observed for *grk*, the anterior enrichment of *bcd* mRNA was reduced in Egl_2pt mutants and virtually eliminated in Egl_4e mutants (Fig. 7G-I,L).

Finally, we examined the localization of *dok* and *sry-α* in oocytes and embryos. These mRNAs were identified as Egl cargoes by the Suter lab and our results are consistent with their findings (Vazquez-Pianzola et al., 2017) (Fig. 1C,D). Both *dok* and *sry-α* are enriched within the oocyte of early-stage wild-type egg chambers (Vazquez-Pianzola et al., 2017) (Fig. S2K,N). This localization pattern was compromised in egg chambers expressing Egl_2pt or Egl_4e (Fig. S2L-P). In addition to the oocyte, both mRNAs are also localized to the apical surface of blastoderm embryos (Vazquez-Pianzola et al., 2017). Our probe set against *dok* revealed an apical enrichment pattern in only a subset of blastoderm embryos (data not shown). Therefore, we focused our analysis on the localization of *sry-α*. Consistent with published results, *sry-α* was strongly localized at the apical surface of embryos expressing wild-type Egl (Vazquez-Pianzola et al., 2017) (Fig. 7M,P). By contrast, this enrichment was greatly reduced in Egl_2pt mutants and was completely disrupted in embryos expressing Egl_4e (Fig. 7N-P).
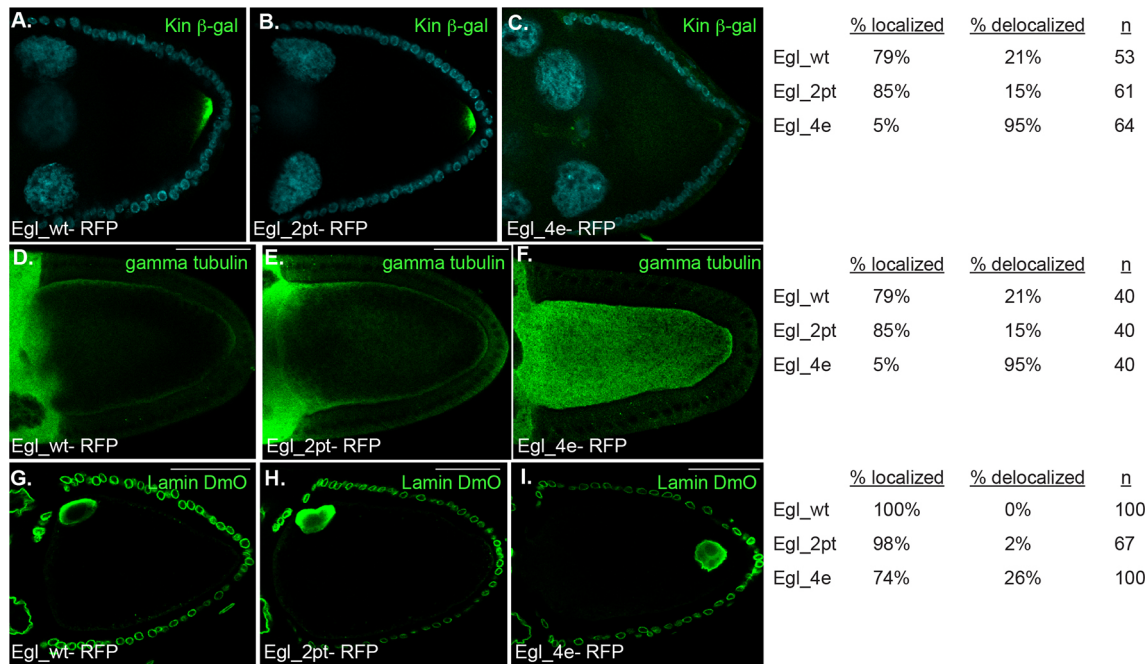
	% localized	% delocalized	n
Egl_wt	79%	21%	53
Egl_2pt	85%	15%	61
Egl_4e	5%	95%	64

	% localized	% delocalized	n
Egl_wt	79%	21%	40
Egl_2pt	85%	15%	40
Egl_4e	5%	95%	40

	% localized	% delocalized	n
Egl_wt	100%	0%	100
Egl_2pt	98%	2%	67
Egl_4e	74%	26%	100

Fig. 6. Microtubules are disorganized in Egl_4e mutants. (A-C) Strains co-expressing Egl_wt-RFP, Egl_2pt-RFP or Egl_4e-RFP and Kinesin-β-gal were fixed and processed for immunofluorescence using an antibody against β-gal (green). (D-I) Ovaries from strains expressing Egl_wt-RFP, Egl_2pt-RFP or Egl_4e-RFP and depleted of endogenous Egl were fixed and processed for immunofluorescence using an antibody against gamma tubulin (D-F) and Lamin DmO (G-I). Phenotype quantifications are indicated on the right.

The severe localization defects observed for *grk*, *bcd* and *sry-α* in Egl_4e mutants are likely to be caused by the disorganized microtubule architecture present in these egg chambers. By contrast, because microtubules appear to be correctly organized in Egl_2pt mutants, the mRNA localization defects in these oocytes and embryos likely result from inefficient binding of Egl to these mRNA cargoes. As such, their association with the Dynein motor is reduced and their localization is compromised.

In conclusion, our results indicate that Dlc-mediated dimerization of Egl is required for optimal RNA binding. Once Egl is bound to RNA cargo, it is then able to interact more efficiently with BicD and the Dynein motor.

DISCUSSION
Dlc is required for Egl dimerization and RNA binding
Egl has been known to physically interact with Dlc for many years (Navarro et al., 2004). However, the significance of this interaction has remained unknown. Egl and Dlc are both required for specification of the oocyte. Genetic loss of either of these gene products arrests oogenesis at early stages (Theurkauf et al., 1993; Carpenter, 1994; Navarro et al., 2004). As such, classical genetic approaches could not be used to study mRNA localization in these mutant backgrounds. In a recent study, we described a strategy to overcome this limitation (Sanghavi et al., 2016). By using shRNA-mediated depletion and a germline driver that is only expressed after oocyte specification, we were able to generate mid- and late-stage egg chambers that were depleted of endogenous Egl. This revealed that Egl was required for localization of *osk*, *bcd* and *grk* mRNAs in the oocyte (Sanghavi et al., 2016). In this report, we used a similar strategy to examine the role of the Egl/Dlc interaction in oocytes and embryos.

The Egl_2pt mutant is compromised for binding to Dlc (Fig. 1) (Navarro et al., 2004). Our findings indicate that Dlc is primarily required for Egl dimerization and that Egl dimerization is linked to its RNA binding activity (Figs 1 and 2). If Egl is unable to dimerize,

it binds RNA localization sequences less efficiently. Consistent with our hypothesis, artificial dimerization of Egl_2pt restored RNA binding and, consequently, the ability of this mutant to interact with BicD (Fig. 3).

Lack of dimerization does not cause Egl to promiscuously interact with non-specific RNAs. The background binding of Egl_wt and Egl_2pt to *ILS-AS* is similar (Figs 1E and 3C,C′). In addition, using native ovarian lysates, gamma tubulin, a non-localizing mRNA, was detected at similar levels in Egl_wt and Egl_2pt pellets (Fig. 1C). This suggests that the overall specificity of Egl_2pt for localization elements is not significantly affected. However, its ability to bind these elements is reduced. In fact, artificial dimerization may further stimulate the RNA binding activity of wild-type Egl. Egl_wt-zip is able to interact more efficiently with *ILS* than a similar wild-type construct that lacks the leucine zipper (Fig. 3C,C′). Despite this increased affinity, the selectivity for the localization element is maintained (Fig. 3C,C′).

The role of BicD in Egl/RNA binding
Consistent with previous results (Mach and Lehmann, 1997), the Egl_4e mutant is deficient in binding to BicD (Fig. 1B). It should be noted, however, that the deficit we observed in our experiments is not as severe as that observed by Mach and Lehmann (Mach and Lehmann, 1997). One possible reason for this difference is that our strategy involves expression of a mutant construct in egg chambers that are depleted of endogenous Egl. Because the driver we used is not active at all stages of egg chamber maturation, the depletion of Egl is incomplete in total ovarian lysates (Sanghavi et al., 2016). The remaining endogenous Egl could dimerize with Egl_4e and thus permit residual binding to BicD.

Our results indicate that Dlc-mediated Egl dimerization promotes RNA binding by Egl and subsequent binding of this complex to BicD. However, the Egl_4e mutant is also compromised for binding RNA (Fig. 1C-E). One explanation for this phenotype is that Egl_4e is
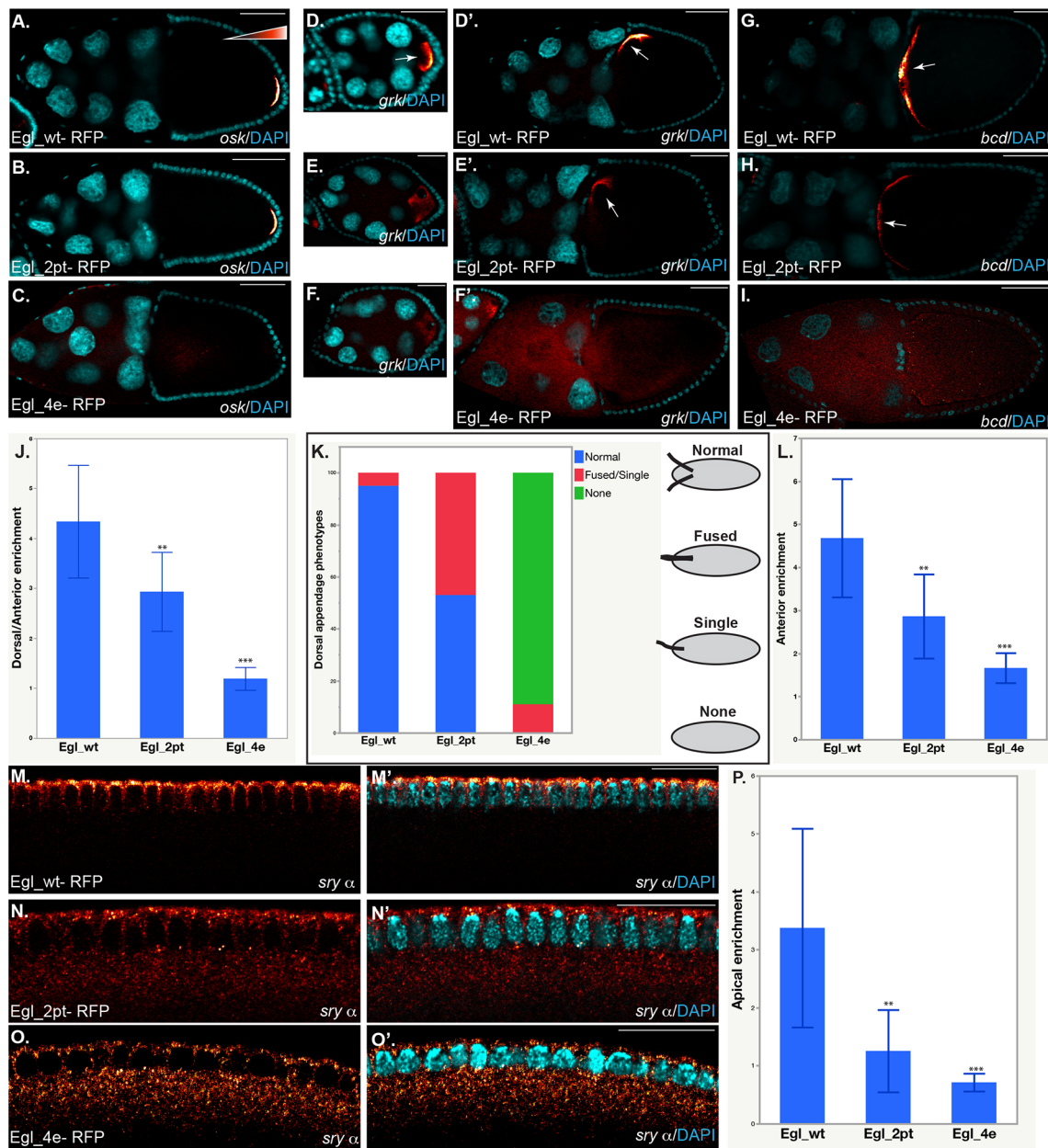
DEVELOPMENT

Fig. 7. RNA localization in Egl wild-type and mutant backgrounds. (A-I) Single molecule FISH (smFISH) analysis of ovaries from strains expressing Egl_wt-RFP, Egl_2pt-RFP or Egl_4e-RFP and depleted of endogenous Egl using probes against *osk* (A-C), *grk* (D-F) or *bcd* mRNA (G-I). Arrows indicate *grk* mRNA enriched within the oocyte of early-stage egg chambers (D), *grk* mRNA localized at the dorsal-anterior cortex of stage 10 egg chambers (D′,E′) or *bcd* mRNA localized at the anterior of the oocyte in stage 10 egg chambers (G,H). (J) The dorsal-anterior enrichment of *grk* mRNA was quantified in strains expressing Egl_wt-RFP, Egl_2pt-RFP and Egl_4e-RFP; *n*=10. (K) The dorsal appendage phenotype in mature eggs from these strains was scored; *n*=100. (L) The anterior enrichment of *bcd* in these strains was quantified; *n*=10. (M-O′) smFISH analysis of embryos from strains expressing Egl_wt-RFP, Egl_2pt-RFP and Egl_4e-RFP using probes against *sry-α* (M-O) and counterstained with DAPI (M′-O′). (P) The apical enrichment of *sry-α* in these embryos was quantified, *n*=10 for Egl_wt and Egl_2pt and *n*=7 for Egl_4e. *In situ* signal is depicted using a red-to-white lookup table; red represents low-intensity signal and white represents high-intensity signal. To visualize the delocalized signal in Egl_4e egg chambers and embryos, these samples had to be imaged using a higher gain setting than was used to image the wild-type control. Data are mean±s.d. ***P<0.001, **P<0.05 (unpaired *t*-test). Scale bars: 25 µm in D,E,F; 50 µm in A-C,D′-I,M-O′.

misfolded and represents a loss-of-function mutation. Consistent with this possibility, microtubules are disorganized in Egl_4e-expressing egg chambers (Fig. 6). However, Egl_4e retains that ability to interact with Dlc (Fig. 1B,B′). This argues against complete misfolding. However, it is possible that Egl_4e is misfolded in a manner that compromises RNA binding and microtubule organization, yet preserves the ability of the protein to interact with Dlc.

Another explanation for this phenotype is that in addition to Dlc, BicD is also required for stable association of Egl with RNA localization sequences. Dienstbier and colleagues noted that recombinant Egl purified from *Saccharomyces cerevisiae* required the addition of BicD in order to bind RNA localization elements (Dienstbier et al., 2009). Based on these published findings and our current results, we hypothesized that BicD might be required to

stabilize the Egl/RNA complex *in vivo*. If our hypothesis is correct, wild-type Egl will not remain bound to RNA in the absence of BicD. We attempted to test this hypothesis by depleting BicD. Although BicD could be efficiently depleted, this treatment resulted in disorganized egg chambers (Fig. S2Q-U). In addition, depletion of BicD severely compromised the expression level of wild-type Egl (Fig. S2R). As such, we were not able to test our hypothesis.

Formation of a transport complex

Using purified proteins, the Bullock and Trybus labs recently demonstrated that a minimal complex consisting of an RNA-localization element, Egl, BicD, Dynactin and Dynein was sufficient for processive minus end movement (McClintock et al., 2018; Sladewski et al., 2018). These studies also indicated that the presence of RNA stimulated the Egl-BicD interaction and that the majority of fast-moving complexes contained two copies of Egl (McClintock et al., 2018; Sladewski et al., 2018). Our results are consistent with these findings and indicate that before binding RNA and BicD, Egl is first dimerized with the help of Dlc. Our results also indicate that disrupting the Egl/Dlc interaction affects formation of this minimal transport complex.

The main difference between our findings and the conclusions drawn by the aforementioned *in vitro* studies has to do with the role of Dlc in RNA transport. Using purified complexes containing either wild-type or Egl_2pt (McClintock et al., 2018), or using Dynein complexes lacking Dlc (Sladewski et al., 2018), the authors conclude that Dlc is neither required for linking the Egl/RNA complex with Dynein, nor is it required for transport of said cargo. Although true under *in vitro* conditions using purified proteins, the situation *in vivo*, as reflected by our findings, indicates an important role for Dlc in this process. In the complex environment of the cell, Dlc is required for Egl dimerization and consequently for RNA binding. Thus, although Dlc is not required for linking the Egl/RNA complex with Dynein, it is required at an earlier step; formation of a localization-competent transport particle. Consistent with this notion, wild-type Egl co-localizes with microtubule filaments in the cytoplasm of nurse cells (Fig. 4A-C). By contrast, Egl_2pt is localized in a diffuse cytoplasmic pattern with only residual filament localization (Fig. 4D).

The net result of disrupting the Egl/Dlc interaction is defective mRNA localization (Fig. 7). *grk*, *bcd* and *sry-α* were inefficiently localized in Egl_2pt mutants. It is likely that the same phenotype would also be observed for other Dhc-localized mRNA cargo. These findings are consistent with previous results obtained using *egl³ᵉ* mutants (Navarro et al., 2004; Bullock et al., 2006). Egl³ᵉ is partially defective for binding to Dlc (Navarro et al., 2004).

Although *grk*, *bcd* and *sry-α* were not efficiently localized in *egl_2pt* mutants, they were not completely delocalized either. This suggests that the residual RNA binding activity of Egl_2pt might be sufficient to couple a certain fraction of these cargo molecules to Dynein. However, this might not be true for all cargoes. For example, cargoes localized during early stages of egg chamber development might be particularly sensitive to disruption of the Egl/Dlc interaction. In early-stage egg chambers, the oocyte enrichment of Egl_2pt is significantly compromised (Fig. 6C). Thus, cargoes localized during this time frame will likely not be correctly sorted. In this regard, it is interesting to note that flies homozygous for *egl_2pt* do not form mature eggs (Navarro et al., 2004). Rather, maturation is halted and oocyte fate is not maintained. It is possible that certain essential cargoes that are transported by Egl and Dynein are not correctly localized in this background, resulting in an oogenesis block. Additional studies might reveal the identity of these cargoes.

Another class of cargo that might be highly sensitive to disruption of the Egl/Dlc interaction are cargoes that are not actively anchored at their site of localization. Both *grk* and *bcd* mRNAs have well-defined anchoring mechanisms (Delanoue et al., 2007; Weil et al., 2008; Trovisco et al., 2016). Thus, in the case of these mRNAs, even if transport is not that efficient, the presence of an anchoring mechanism can lessen the severity of the localization defect. Cargoes without such an anchoring mechanism would be significantly more delocalized.

Model

Based on these results, and on the recent findings of the Bullock and Trybus labs (McClintock et al., 2018; Sladewski et al., 2018), we propose the following model (Fig. 8). Dlc is required for dimerization of Egl. Dimeric Egl is able to more efficiently associate with RNA cargo that is destined for localization. Cargo association
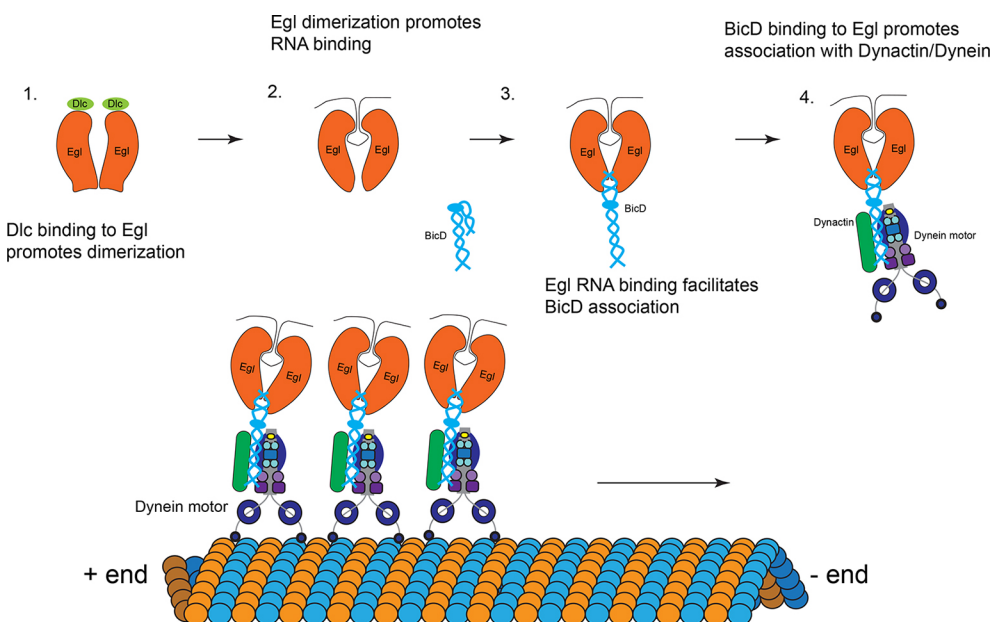

Fig. 8. A model to illustrate the mechanism by which Dlc and BicD function to link the Egl/mRNA complex to the Dynein motor. Dlc is required for dimerization of Egl. Once dimerized, Egl is able to efficiently bind RNA and interact with BicD. This relieves the auto-inhibition of BicD and enables the complex to associate with the Dynein motor.

DEVELOPMENT

in turn promotes the interaction of Egl with BicD, an adaptor for the Dynein motor. As such, disrupting the Egl/Dlc interaction results in mRNA being inefficiently associated with Dynein, and therefore incompletely localized within the cell.

MATERIALS AND METHODS

Fly stocks

The following stocks were used: Oregon-R-C and w[1118] were used as wild-type [Bloomington *Drosophila* Stock Center (BDSC); #5 and #5905, respectively]. The shRNA strains were: *eb1* shRNA (BDSC; #36680, donor TRiP); *white* shRNA (BDSC; #35573, donor TRiP); *egl* shRNA-1 (BDSC; #43550, donor TRiP); *ctp/lc8* shRNA (BDSC; #42862, donor TRiP). shRNA expression was driven using either P{w[+mC]=matalpha4-GAL-VP16}V37 (BDSC, #7063; donor Andrea Brand) for early-stage expression or w[*]; P{w[+mC]=matalpha4-GAL-VP16}V2H (BDSC, #7062; donor Andrea Brand) for mid-stage expression. Egl_wt-RFP, Egl_2pt-RFP, Egl_4e-RFP and Khc-RFP transgenes were constructed by cloning the respective coding regions into the pattB vector (Bischof et al., 2007). All four alleles were inserted at the attP1 site (BDSC, #34760) (Ni et al., 2009). The transgenic strains were injected by BestGene. Microtubule plus ends were marked using the Kin:βgal strain (Clark et al., 1994). Fly stocks and crosses used for these experiments were maintained at 25°C.

Antibodies

The following antibodies were used for immunofluorescence: rat anti-RFP (Chromotek, clone 5F8, 1:1000); mouse anti-Dhc [Developmental Studies Hybridoma Bank (DHSB), clone 2C11-2, 1:250; donor J. Scholey, University of California, Davis]; mouse anti-BicD (Clones 1B11 and 4C2, DHSB, 1:300; donor R. Steward, Waksman Institute, Rutgers University); mouse anti-β-galactosidase (Promega, Z3781, 1:2000); mouse anti-γ-tubulin (Sigma-Aldrich, T5326, 1:100); mouse anti-LaminDmO (DHSB, clone ADL84.12, 1:200; donor P. A. Fisher, Pharmacological Sciences, SUNY at Stony Brook); alpha-tubulin FITC (Sigma-Aldrich, F2168, 1:150); goat anti-rat Alexa 594 (Life Technologies, A-11007, 1:400); goat anti-rabbit Alexa 594 and 488 (Life Technologies, A-11012 and A-11008, respectively; 1:400 and 1:200, respectively); goat anti-mouse Alexa 594 and 488 (Life Technologies, R37121 and A-11001, respectively; 1:400 and 1:200, respectively). The following antibodies were used for western blotting: rabbit anti-Egl (1:5000, from R. Lehmann, Skirball Institute of Biomolecular Medicine); rabbit anti-Ctp (Abcam, ab51603, 1:5000); mouse anti-GFP (Clontech, JL-8, 1:5000); rat anti-RFP (Chromotek, 5f8-100, 1:4000); mouse anti-BicD (Clones 1B11 and 4C2, DHSB, 1:300 each); anti-FLAG (Sigma-Aldrich, F1804, 1:5000); goat anti-mouse HRP (Pierce, 31430, 1:5000); goat anti-rabbit HRP (Pierce, 31460, 1:5000); goat anti-rat HRP (Pierce, 31470, 1:5000). The following antibodies were used for immunoprecipitation: GST (Santa Cruz Biotechnology, sc-138, 1:15) and mouse anti-BicD (DHSB, clones 1B11 and 4C2 both used together at 1:30). For the experiment shown in Fig. 4, a home-made polyclonal antibody against RFP was used. GST-RFP was used as the antigen. The antigen was injected into rabbits by Pacific Immunology. Subsequently, serum was extracted by Pacific Immunology and shipped to our lab. Antibody specific to RFP was purified using recombinant RFP cross-linked to beads. The purified antibody was eluted and dialyzed into PBS. The specificity of the antibody was tested using egg chambers from either w1118 flies or flies expressing Egl_wt-RFP. The egg chambers were co-stained with α-tubulin FITC. Robust RFP signal is observed in Egl_wt-RFP egg chambers (Fig. S2A,C), but not in w1118 egg chambers (Fig. S2B,D).

DNA constructs

The transgenes for expressing Egl_wt, Egl_2pt, Egl_4e and Khc in the female germline were constructed by cloning the respective cDNAs into the pAttB vector (Bischof et al., 2007). The mutations were made using the Q5 Site-Directed Mutagenesis Kit (New England Biolabs). The constructs contained the promoter from the maternal α-tubulin gene, a C-terminal RFP tag and the 3′UTR from the *vasa* gene. Two silent mutations were introduced into the constructs in order to make them refractory to the *egl* shRNA. In addition, a flexible linker was present

in between the gene of interest and the RFP tag. The constructs were engineered using Gibson assembly (New England Biolabs). For expression in S2 cells, the same constructs were cloned into the pUASp-attB-K10 vector (Bischof et al., 2007) upstream of either a GFP, RFP or 3×FLAG tag. The constructs were expressed in S2 cells by co-transfecting along with an Act5c-Gal4 plasmid (gift from Jocelyn McDonald, Kansas State University). The leucine zipper from GCN4 (AAL09032.1) along with a preceding flexible linker sequence was synthesized with *Drosophila* codon optimization by Genewiz.

Cell culture

The S2 cells used in this study were obtained from the *Drosophila* Genomics Resource Center. The cells correspond to the S2-DRSC line (stock number 181). The cells were grown in Schneider's medium containing 10% heat inactivated fetal calf serum. S2 cells were transfected using Effectene (Qiagen) according to the instructions provided by the manufacturer.

Analyzing protein-protein interaction

Ovaries from the indicated genotypes were dissected and flash frozen in liquid nitrogen until ready to use. The ovaries were homogenized into lysis buffer [50 mM Tris (pH 7.5), 50 mM NaCl, 0.2 mM EDTA, 0.05% NP40 and Halt protease inhibitor cocktail (Pierce)] and cleared by centrifugation at 10,000 *g* at 4°C for 5 min. Between 800 µg and 1000 µg total protein was used per immunoprecipitation. For ovarian lysates, immunoprecipitation was performed by incubating the lysates at 4°C for 1 h with RFP-trap beads (Chromotek). Subsequently, the beads were washed four times with wash buffer [50 mM Tris (pH 7.5), 200 mM NaCl, 0.2 mM EDTA, 0.05% NP40]. The co-precipitating proteins were eluted in Laemmli buffer, run on a gel and analyzed by western blotting. For examining protein-protein interaction using S2 cells, lysates were prepared using the indicated transfected cells. Lysis was performed using RIPA buffer [50 mM Tris-Cl (pH 7.5), 150 nM NaCl, 1% NP40, 1 mM EDTA]. The lysates were cleared by centrifugation as described above and added to GFP-trap beads.

Analyzing *in vivo* protein-mRNA association

In order to examine binding to native mRNAs, ovaries were dissected and stored as described above. Then, 0-8 h embryos were collected, dechorionated and flash frozen in liquid nitrogen. Between 800 µg and 1000 µg of ovarian or embryonic lysate was used per immunoprecipitation. The tagged proteins were immunoprecipitated using RFP-Trap beads using a previously described protocol (Sanghavi et al., 2016). The co-precipitating RNAs were reverse transcribed using random hexamers and Superscript III (Life Technologies) according to the manufacturer's instructions. Each quantitative PCR reaction used 167 ng of cDNA (except for reactions with *grk* mRNA: 267 ng) using the SsoAdvanced Universal SYBR Green Supermix (Bio-Rad) and a Bio-Rad CFX96 Real-Time PCR System. Fold enrichment was calculated by comparing ct values for each RNA with that obtained for γ-tubulin.

The following primers were used: *bcd* mRNA (5′-AATCGGAT-CAGCACAAGGAC-3′ and 5′-GCGTTGAATGACTCGCTGTA-3′), *grk* mRNA (5′-ATCCGATGGTGAACAACACA-3′ and 5′-CGACGACAGC-ATGAGGAGTA-3′), *nos* mRNA(5′-TGTGGCGAAACATGTCGTAT-3′ and 5′-TCTCACAAAGACGCAGTGG-3′), *pgc* mRNA (5′-ACCCGAA-AATGTGCGACTAC-3′ and 5′-ATCTCCATCTATCCGCGATG-3′), *sry-α* mRNA (5′-GCAGTGAGCTGATTGCAGAG-3′ and 5′-AGGTGGGTG-ATGCAGGTTAC-3′), *dok* mRNA (5′-ATGTCCGCCAAGATGAAGTC-3′ and 5′-GATATGCAGCTTTGCGTTGA-3′) and *γ-tubulin* mRNA (5′-CCACCATCATGAGTCTGAGC-3′ and 5′-ACCGATGAGGTTGTTG-TTCA-3′).

In vitro protein/RNA interaction

ILS, *ILS-AS* and *TLS* constructs containing a T7 transcription site and an aptamer with high affinity for streptavidin was obtained from Simon Bullock (MRC Laboratory of Molecular Biology, Cambridge, UK; Dix et al., 2013). The constructs were transcribed and purified as previously described (Dix et al., 2013). The RNA affinity purification was also performed as previously described, with a few modifications (Dix et al., 2013). First, 5 µg of RNA was refolded in 10 µl of *Drosophila* extraction buffer [DXB: 25 mM HEPES (pH 6.5), 50 mM KCl, 1 mM MgCl₂,

250 mM sucrose, 0.1% NP40, supplemented with 10 μM MgATP and 1 mM DTT at the time of use]. Refolding was accomplished using a Bio-Rad C1000 Thermo Cycler with the following protocol: 56°C/5 min, 37°C/10 min, 25°C/10 min. The refolded RNA was then incubated with High Capacity Streptavidin Agarose Beads (Pierce) in 90 μl DXB for 1.5 h at 4°C while nutating. Extracts were prepared from either frozen *Drosophila* ovaries or dechorionated embryos in lysis buffer [50 mM Tris (pH 7.5), 50 mM NaCl, 0.2 mM EDTA, 0.05% NP40 and Halt protease inhibitor cocktail (Pierce)] using a sanitized pestle or in RIPA buffer [50 mM Tris (pH 7.5), 200 mM NaCl, 0.2 mM EDTA, 0.05% NP40] for S2 cells. Halt Protease Inhibitor mix (Thermo Fisher Scientific) and RNaseOUT (Life Technologies) were added to the extracts. The beads were rinsed twice with the above lysis buffer before the addition of extracts. Typically between 800 μg and 1000 μg of total protein was used in each binding experiment. The extracts were incubated with the RNA-bound streptavidin beads for 15 min at room temperature and a further 30 min at 4°C with nutation. The beads were then rinsed four times in lysis buffer, the bound proteins were eluted by boiling in Laemmli buffer and examined by western blotting.

Immunofluorescence

Before dissection, flies were fattened on yeast pellets for 3 days. Ovaries were dissected as previously described (Liu et al., 2015) and fixed in 4% formaldehyde (Pierce) for 20 min at room temperature. The fixative was diluted in PBS. The immunofluorescence staining was performed as previously described (Liu et al., 2015). The primary antibody was incubated in 1× PBST (PBS+0.1% Triton X-100)+0.2% bovine serum albumin (BSA) (Promega) overnight at 4°C. The next day, the samples were washed three times in PBST. The secondary antibody was diluted in 1× PBST+0.2% BSA and incubated overnight at 4°C. The following day, the ovaries were washed three times in PBST, mounted on slides with Aqua-Poly/Mount (APM, Polysciences) and imaged. In order to detect Egl and microtubule filaments, dissected ovaries were incubated in PIPES buffer (80 mM PIPES, 1 mM EGTA, 1 mM MgCl$_2$, 0.1% Triton X-100) for 1 h without agitation. The ovaries were subsequently fixed in 4% formaldehyde for 20 min at room temperature. The fixative was removed, the ovaries were washed once with PBST and then incubated for 1 h in 100% methanol at −20°C. The ovaries were gradually rehydrated into PBST and processed for immunofluorescence staining as described above.

In situ hybridization

Before dissection, flies were fattened on yeast pellets for 3 days. Dissected ovaries and dechorionated embryos were fixed with 4% formaldehyde for 20 min. Next, the fixative was removed and the ovaries were washed with PBST. Ovaries were further teased apart using a pipette. The ovaries or embryos were washed with 100% methanol for 5 min, then stored for at least 1 h in 100% methanol at −20°C. The samples were then re-hydrated with three 10 min washes with a solution of PBST and 100% methanol (3:7, 1:1, 7:3) and rinsed four times with PBST. The samples were then washed for 10 min in wash buffer [4× saline-sodium citrate (SSC), 35% deionized formamide, 0.1% Tween-20]. Fluorescent probes were diluted in hybridization buffer [10% dextran sulfate, 0.1 mg/ml salmon sperm ssDNA, 100 μl vanadyl ribonucleoside (New England Biolabs), 20 μg/ml RNAse-free BSA, 4× SSC, 0.1% Tween-20, 35% deionized formamide] and were applied overnight at 37°C. The following day, the samples were washed twice with pre-warmed wash buffer for 30 min. After two rinses with PBST and two rinses with PBS, the ovaries or embryos were mounted on slides using APM and imaged.

Microscopy

Images were captured using a Zeiss LSM 780 upright microscope and processed for presentation using Fiji, Adobe Photoshop and Adobe Illustrator. All imaging experiments were performed at the Augusta University Cell Imaging Core.

Quantification

Quantifications of localized RNAs and proteins were carried out by measuring the average pixel intensity of the localized signal and dividing by the delocalized signal. For *grk* and *bcd*, the localized signal at the dorsal-

anterior (*grk*) of the oocyte or at the anterior margin (*bcd*) of the oocyte was compared with the delocalized signal in the rest of the oocyte. For *sry-α*, the localized signal above the blastoderm nuclei was compared with the delocalized signal below the nuclei. For quantifying Egl and Dhc oocyte enrichment, the signal in the oocyte was compared with the delocalized signal in the rest of the egg chamber. Quantifications were performed using Zeiss Zen Black software. In order to calculate the co-localization coefficient between Egl and microtubule filaments, the Coloc2 plugin on Fiji/ImageJ was used. An unpaired *t*-test was performed using s.d., mean and the *n* value.

Author contributions

Conceptualization: C.H.G., H.N., R.V.-K., G.B.G.; Methodology: C.H.G., H.N., R.V.-K., G.B.G.; Formal analysis: C.H.G., H.N., R.V.-K., G.B.G.; Investigation: C.H.G., H.N., R.V.-K., G.B.G.; Writing - original draft: C.H.G.; Writing - review & editing: C.H.G., H.N., G.B.G.; Supervision: G.B.G.; Project administration: G.B.G.; Funding acquisition: G.B.G.

Supplementary information

Supplementary information available online at
http://dev.biologists.org/lookup/doi/10.1242/dev.176529.supplemental

References

Barbar, E. (2008). Dynein light chain LC8 is a dimerization hub essential in diverse protein networks. *Biochemistry* **47**, 503-508. doi:10.1021/bi701995m

Berleth, T., Burri, M., Thoma, G., Bopp, D., Richstein, S., Frigerio, G., Noll, M. and Nüsslein-Volhard, C. (1988). The role of localization of bicoid RNA in organizing the anterior pattern of the Drosophila embryo. *EMBO J.* **7**, 1749-1756. doi:10.1002/j.1460-2075.1988.tb03004.x

Bischof, J., Maeda, R. K., Hediger, M., Karch, F. and Basler, K. (2007). An optimized transgenesis system for Drosophila using germ-line-specific phiC31 integrases. *Proc. Natl. Acad. Sci. USA* **104**, 3312-3317. doi:10.1073/pnas.0611511104

Bullock, S. L. and Ish-Horowicz, D. (2001). Conserved signals and machinery for RNA transport in Drosophila oogenesis and embryogenesis. *Nature* **414**, 611-616. doi:10.1038/414611a

Bullock, S. L., Nicol, A., Gross, S. P. and Zicha, D. (2006). Guidance of bidirectional motor complexes by mRNA cargoes through control of dynein number and activity. *Curr. Biol.* **16**, 1447-1452. doi:10.1016/j.cub.2006.05.055

Cajigas, I. J., Tushev, G., Will, T. J., tom Dieck, S., Fuerst, N. and Schuman, E. M. (2012). The local transcriptome in the synaptic neuropil revealed by deep sequencing and high-resolution imaging. *Neuron* **74**, 453-466. doi:10.1016/j.neuron.2012.02.036

Carpenter, A. T. (1994). Egalitarian and the choice of cell fates in Drosophila melanogaster oogenesis. *Ciba Found Symp* **182**, 223-246. doi:10.1002/9780470514573.ch13

Cha, B.-J., Serbus, L. R., Koppetsch, B. S. and Theurkauf, W. E. (2002). Kinesin I-dependent cortical exclusion restricts pole plasm to the oocyte posterior. *Nat. Cell Biol.* **4**, 592-598. doi:10.1038/ncb832

Cho, A., Kato, M., Whitwam, T., Kim, J. H. and Montell, D. J. (2016). An atypical tropomyosin in drosophila with intermediate filament-like properties. *Cell Rep.* **16**, 928-938. doi:10.1016/j.celrep.2016.06.054

Clark, I., Giniger, E., Ruohola-Baker, H., Jan, L. Y. and Jan, Y. N. (1994). Transient posterior localization of a kinesin fusion protein reflects anteroposterior polarity of the Drosophila oocyte. *Curr. Biol.* **4**, 289-300. doi:10.1016/S0960-9822(00)00068-3

Delanoue, R., Herpers, B., Soetaert, J., Davis, I. and Rabouille, C. (2007). Drosophila Squid/hnRNP helps Dynein switch from a gurken mRNA transport motor to an ultrastructural static anchor in sponge bodies. *Dev. Cell* **13**, 523-538. doi:10.1016/j.devcel.2007.08.022

Dick, T., Ray, K., Salz, H. K. and Chia, W. (1996). Cytoplasmic dynein (ddlc1) mutations cause morphological defects and apoptotic cell death in Drosophila melanogaster. *Mol. Cell. Biol.* **16**, 1966-1977. doi:10.1128/MCB.16.5.1966

DEVELOPMENT

Dienstbier, M., Boehl, F., Li, X. and Bullock, S. L. (2009). Egalitarian is a selective RNA-binding protein linking mRNA localization signals to the dynein motor. *Genes Dev.* **23**, 1546-1558. doi:10.1101/gad.531009

Dix, C. I., Soundararajan, H. C., Dzhindzhev, N. S., Begum, F., Suter, B., Ohkura, H., Stephens, E. and Bullock, S. L. (2013). Lissencephaly-1 promotes the recruitment of dynein and dynactin to transported mRNAs. *J. Cell Biol.* **202**, 479-494. doi:10.1083/jcb.201211052

Ephrussi, A., Dickinson, L. K. and Lehmann, R. (1991). Oskar organizes the germ plasm and directs localization of the posterior determinant nanos. *Cell* **66**, 37-50. doi:10.1016/0092-8674(91)90137-N

Goldman, C. H. and Gonsalvez, G. B. (2017). The role of microtubule motors in mRNA localization and patterning within the drosophila oocyte. *Results Probl. Cell Differ.* **63**, 149-168. doi:10.1007/978-3-319-60855-6_7

Hoogenraad, C. C., Akhmanova, A., Howell, S. A., Dortland, B. R., De Zeeuw, C. I., Willemsen, R., Visser, P., Grosveld, F. and Galjart, N. (2001). Mammalian Golgi-associated Bicaudal-D2 functions in the dynein-dynactin pathway by interacting with these complexes. *EMBO J.* **20**, 4041-4054. doi:10.1093/emboj/20.15.4041

Kardon, J. R. and Vale, R. D. (2009). Regulators of the cytoplasmic dynein motor. *Nat. Rev. Mol. Cell Biol.* **10**, 854-865. doi:10.1038/nrm2804

Kim-Ha, J., Smith, J. L. and Macdonald, P. M. (1991). oskar mRNA is localized to the posterior pole of the Drosophila oocyte. *Cell* **66**, 23-35. doi:10.1016/0092-8674(91)90136-M

Lecuyer, E., Yoshida, H., Parthasarathy, N., Alm, C., Babak, T., Cerovina, T., Hughes, T. R., Tomancak, P. and Krause, H. M. (2007). Global analysis of mRNA localization reveals a prominent role in organizing cellular architecture and function. *Cell* **131**, 174-187. doi:10.1016/j.cell.2007.08.003

Li, M., McGrail, M., Serr, M. and Hays, T. S. (1994). Drosophila cytoplasmic dynein, a microtubule motor that is asymmetrically localized in the oocyte. *J. Cell Biol.* **126**, 1475-1494. doi:10.1083/jcb.126.6.1475

Liu, G., Sanghavi, P., Bollinger, K. E., Perry, L., Marshall, B., Roon, P., Tanaka, T., Nakamura, A. and Gonsalvez, G. B. (2015). Efficient endocytic uptake and maturation in drosophila oocytes requires dynamitin/p50. *Genetics* **201**, 631-649. doi:10.1534/genetics.115.180018

Mach, J. M. and Lehmann, R. (1997). An egalitarian-BicaudalD complex is essential for oocyte specification and axis determination in Drosophila. *Genes Dev.* **11**, 423-435. doi:10.1101/gad.11.4.423

McClintock, M. A., Dix, C. I., Johnson, C. M., McLaughlin, S. H., Maizels, R. J., Hoang, H. T. and Bullock, S. L. (2018). RNA-directed activation of cytoplasmic dynein-1 in reconstituted transport RNPs. *Elife* **7**. doi:10.7554/eLife.36312

McGrail, M. and Hays, T. S. (1997). The microtubule motor cytoplasmic dynein is required for spindle orientation during germline cell divisions and oocyte differentiation in Drosophila. *Development* **124**, 2409-2419.

McKenney, R. J., Huynh, W., Tanenbaum, M. E., Bhabha, G. and Vale, R. D. (2014). Activation of cytoplasmic dynein motility by dynactin-cargo adapter complexes. *Science* **345**, 337-341. doi:10.1126/science.1254198

Mili, S., Moissoglu, K. and Macara, I. G. (2008). Genome-wide screen reveals APC-associated RNAs enriched in cell protrusions. *Nature* **453**, 115-119. doi:10.1038/nature06888

Navarro, C., Puthalakath, H., Adams, J. M., Strasser, A. and Lehmann, R. (2004). Egalitarian binds dynein light chain to establish oocyte polarity and maintain oocyte fate. *Nat. Cell Biol.* **6**, 427-435. doi:10.1038/ncb1122

Neuman-Silberberg, F. S. and Schupbach, T. (1993). The Drosophila dorsoventral patterning gene gurken produces a dorsally localized RNA and encodes a TGF alpha-like protein. *Cell* **75**, 165-174. doi:10.1016/S0092-8674(05)80093-5

Ni, J.-Q., Liu, L.-P., Binari, R., Hardy, R., Shim, H.-S., Cavallaro, A., Booker, M., Pfeiffer, B. D., Markstein, M., Wang, H. et al. (2009). A Drosophila resource of transgenic RNAi lines for neurogenetics. *Genetics* **182**, 1089-1100. doi:10.1534/genetics.109.103630

Rapali, P., Szenes, A., Radnai, L., Bakos, A., Pal, G. and Nyitray, L. (2011). DYNLL/LC8: a light chain subunit of the dynein motor complex and beyond. *FEBS J.* **278**, 2980-2996. doi:10.1111/j.1742-4658.2011.08254.x

Ryder, P. V. and Lerit, D. A. (2018). RNA localization regulates diverse and dynamic cellular processes. *Traffic* **19**, 496-502. doi:10.1111/tra.12571

Sanghavi, P., Liu, G., Veeranan-Karmegam, R., Navarro, C. and Gonsalvez, G. B. (2016). Multiple roles for egalitarian in polarization of the drosophila egg chamber. *Genetics* **203**, 415-432. doi:10.1534/genetics.115.184622

Schlager, M. A., Hoang, H. T., Urnavicius, L., Bullock, S. L. and Carter, A. P. (2014). In vitro reconstitution of a highly processive recombinant human dynein complex. *EMBO J.* **33**, 1855-1868. doi:10.15252/embj.201488792

Sladewski, T. E., Billington, N., Ali, M. Y., Bookwalter, C. S., Lu, H., Krementsova, E. B., Schroer, T. A. and Trybus, K. M. (2018). Recruitment of two dyneins to an mRNA-dependent Bicaudal D transport complex. *Elife* **7**. doi:10.7554/eLife.36306

Suter, B. (2018). RNA localization and transport. *Biochim. Biophys. Acta Gene Regul. Mech.* **1861**, 938-951. doi:10.1016/j.bbagrm.2018.08.004

Theurkauf, W. E., Alberts, B. M., Jan, Y. N. and Jongens, T. A. (1993). A central role for microtubules in the differentiation of Drosophila oocytes. *Development* **118**, 1169-1180. doi:10.1016/0168-9525(93)90134-4

Trovisco, V., Belaya, K., Nashchekin, D., Irion, U., Sirinakis, G., Butler, R., Lee, J. J., Gavis, E. R. and St Johnston, D. (2016). bicoid mRNA localises to the Drosophila oocyte anterior by random Dynein-mediated transport and anchoring. *Elife* **5**. doi:10.7554/eLife.17537

Vazquez-Pianzola, P., Schaller, B., Colombo, M., Beuchle, D., Neuenschwander, S., Marcil, A., Bruggmann, R. and Suter, B. (2017). The mRNA transportome of the BicD/Egl transport machinery. *RNA Biol.* **14**, 73-89. doi:10.1080/15476286.2016.1251542

Veeranan-Karmegam, R., Boggupalli, D. P., Liu, G. and Gonsalvez, G. B. (2016). A new isoform of Drosophila non-muscle Tropomyosin 1 interacts with Kinesin-1 and functions in oskar mRNA localization. *J. Cell Sci.* **129**, 4252-4264. doi:10.1242/jcs.194332

Weil, T. T., Parton, R., Davis, I. and Gavis, E. R. (2008). Changes in bicoid mRNA anchoring highlight conserved mechanisms during the oocyte-to-embryo transition. *Curr. Biol.* **18**, 1055-1061. doi:10.1016/j.cub.2008.06.046

Zhao, T., Graham, O. S., Raposo, A. and St Johnston, D. (2012). Growing microtubules push the oocyte nucleus to polarize the Drosophila dorsal-ventral axis. *Science* **336**, 999-1003. doi:10.1126/science.1219147

DEVELOPMENT